Molecular Genetics and Metabolism Reports 33 (2022) 100921

Contents lists available at ScienceDirect

Molecular Genetics and Metabolism Reports

journal homepage: www.elsevier.com/locate/ymgmr

Automated urinary sediment detection for Fabry disease using deep-learning algorithms

Hidetaka Uryu [a,b,1], Ohsuke Migita [c,d,e,1,*], Minami Ozawa [e], Chikako Kamijo [c], Saki Aoto [a], Kohji Okamura [f], Fuyuki Hasegawa [g,h], Torayuki Okuyama [k], Motomichi Kosuga [i,j,k], Kenichiro Hata [d,l]

[a] Medical Genome Center, National Research Institute for Child Health and Development, Tokyo 157-8535, Japan
[b] Department of Leukemia, University of Texas MD Anderson Cancer Center, Houston, TX 77030-4009, USA
[c] Department of Laboratory Medicine, St. Marianna University School of Medicine, Kanagawa 216-8511, Japan
[d] Department of Maternal-Fetal Biology, National Research Institute for Child Health and Development, Tokyo 157-8535, Japan
[e] Department of Pediatrics, St. Marianna University School of Medicine, Kanagawa 216-8511, Japan
[f] Department of Systems BioMedicine, National Research Institute for Child Health and Development, Tokyo 157-8535, Japan
[g] Biobank, National Center for Child Health and Development Research Center, Tokyo 157-8535, Japan
[h] Center for Maternal-Fetal, Neonatal and Reproductive Medicine, National Center for Child Health and Development, Tokyo 157-8535, Japan
[i] Division of Medical Genetics, National Center for Child Health and Development, Tokyo 157-8535, Japan
[j] Department of Clinical Laboratory Medicine, National Center for Child Health and Development, Tokyo 157-8535, Japan
[k] Center for Lysosomal Storage Diseases, National Center for Child Health and Development, Tokyo 157-8535, Japan
[l] Department of Molecuar and Medical Genetics, Gunma University Graduate School of Medicine, Gunma 371-8511, Japan

ARTICLE INFO

Keywords:
Fabry disease
Artificial intelligence
Deep learning
Image augmentation
Mulberry cells

ABSTRACT

Fabry disease is a congenital lysosomal storage disease, and most of these cases develop organ damage in middle age. There are some promising therapeutic options for this disorder, which can stabilize the progression of the disease. However, a long delay in diagnosis prevents early intervention, resulting in treatment failure. Because Fabry disease is a rare disease, it is not well recognized and disease specific screening tests are rarely performed. Hence, a novel approach to for detecting patients with a widely practiced clinical test is crucial for the early detection of the disease. Recently, decision support systems based on artificial intelligence (AI) have been developed in many clinical fields. However, the construction of these models requires datasets from a large number of samples; this aspect is one of the main obstacles in AI-based approaches for rare diseases. In this study, with a novel image amplification method to construct the dataset for AI-model training, we built the deep neural-network model to detect Fabry cases from their urine samples. Sensitivity, specificity, and the AUC of the models on validation dataset were 0.902 (95% CI, 0.900–0.903), 0.977 (0.950–0.980), and 0.968 (0.964–0.972), respectively. This model could also extract disease-specific findings that are interpretable with human recognition. These results indicate that we can apply novel AI models for rare diseases based on this image amplification method we developed. We expect this approach could contribute to the diagnosis of Fabry disease.
Synopsis: This is the first reported AI-based decision support system to detect undiagnosed Fabry cases, and our new image amplification method will contribute to the AI models for other rare disorders.

Abbreviations: AdHE, adaptive histogram equalization; AI, artificial intelligence; alpha-Gal A, α- galactosidase A; AUC, area under the curve; CNN, convolutional neural network; CntStr, contrast stretching; ERT, enzyme replacement therapy; InceptResNet, InceptionResNetV2; OrdHE, ordinary histogram equalization; ROC, receiver operating characteristic; Xcep, Xception.

* Corresponding author at: Department of Laboratory Medicine, St. Marianna University School of Medicine, 2-16-1 Sugao, Miyamae-ku, Kawasaki city, Kanagawa 216-8511, Japan.
E-mail address: migita@marianna-u.ac.jp (O. Migita).

[1] These authors contributed equally to this work.

https://doi.org/10.1016/j.ymgmr.2022.100921
Received 29 May 2022; Received in revised form 21 September 2022; Accepted 22 September 2022

1. Introduction

Fabry disease is the most prevalent lysosomal storage disorder. This disease is inherited as an X-linked disorder and is caused by mutations in the GLA gene encoding the α-galactosidase A (alpha-Gal A) enzyme [1]. The complete or partially deficient activity of this lysosomal enzyme leads to the accumulation of sphingolipids and globosides in many cell types throughout the body, resulting in multiple organ failure [2–4].

The prevalence of this disorder was previously underestimated because its classical form alone was mainly focused upon [5,6]. However, with the better understanding of the disease variants, the prevalence of the disease has been corrected upward and has been estimated to be one in about 1500 to 15,000 people, according to their ethnicity [7–10].

The diagnostic approach for the early detection of Fabry disease without family history is challenging because of the disease rarity, nonspecific symptoms particularly in the early stage of the disease, and the widespread misconceptions of the disease entity [11]. The mean delay for disease diagnosis, from the first visit, was estimated to be approximately 15 years [12], which can result in multiple organ failure. There are certain effective therapeutic options for Fabry disease available, such as enzyme replacement therapy (ERT) or oral pharmacologic chaperone therapy [13–15]. However, these treatments are known to be effective only if they commenced before the progression of organ damage [16,17].

There are several tests to diagnose Fabry patients, such as enzymatic assays for α-Gal A activity in leukocytes, GLA gene mutation analysis, or skin pathology test for globotriaosylceramide accumulation. However, none of these tests can be used as screening tools for disease prevention because of their cost or invasiveness. Thus, more simple diagnostic tools are desired, applicable before disease progression. Recently, the disease-specific urinary findings for Fabry disease, namely mulberry cells or mulberry bodies, have been focused upon for the detection of the early signs of the disease, without being invasive and expensive [18–20]. However, those findings are often unnoticed and seldom lead to the prevention of disease development, mainly because of their low familiarity among general clinicians.

Recently, the application of artificial intelligence (AI), including deep neural network algorithms, has been established as decision support systems in many clinical fields. However, these applications are mainly limited to the diseases with high pretest probabilities, and most of them do not have high accuracy for rare diseases due to their relatively small sample size for model construction [21].

To address these issues, we constructed neural network models that could detect Fabry cases from urine sediment images. We also developed a new image augmentation method to improve the generalization of training data obtained from a relatively small number of original images. This is the first report of an AI model using image enhancement methods to screen for low prevalence metabolic diseases in a generally healthy population. We expect that this screening system will contribute to the early detection of Fabry's disease, as well as other rare disorders.

2. Material and methods

2.1. Patient enrollment

We have selected Fabry cases and control cases retrospectively from the National Center for Child Health and Development (NCCHD) (Tokyo, Japan) and the St. Marianna University School of Medicine (Kawasaki, Japan) records, between January 1, 2011, and September 1, 2018. The Fabry cases were diagnosed definitively before enrollment by a combination of alpha-Gal A activity measurement and variant analysis of the GLA gene. The urine sample images from these enrolled cases are divided into training or validation groups, preprocessed, and collected

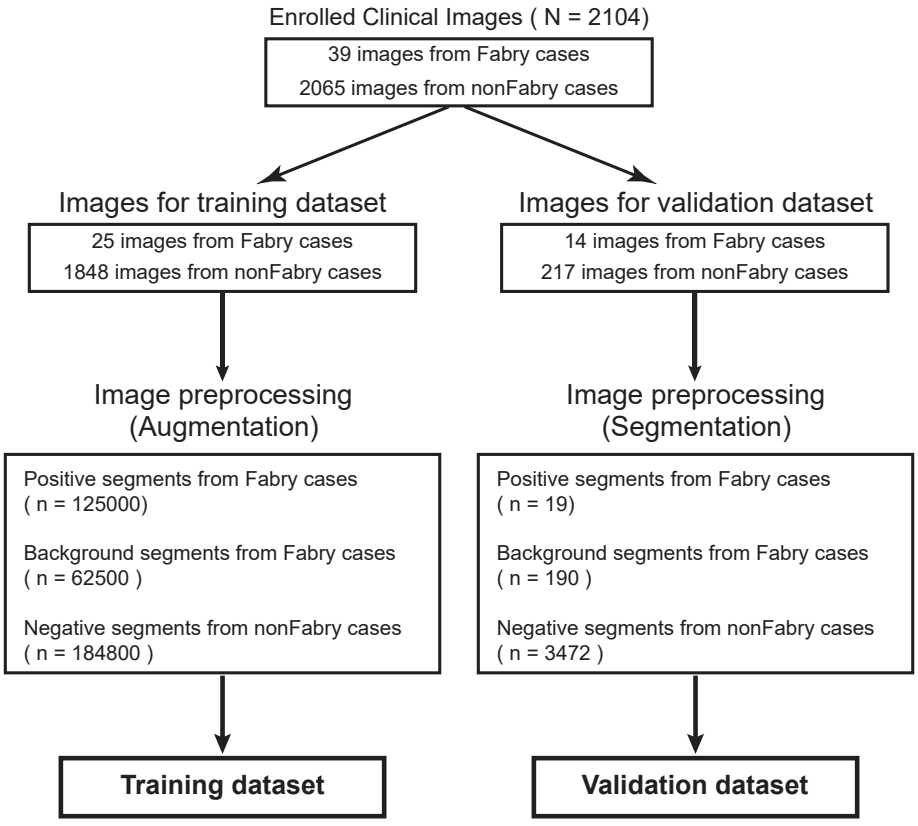

Fig. 1. Training and validation datasets for detecting Fabry disease.
All enrolled images are divided into training or validation groups, preprocessed, and collected in each dataset.

in the training or validation dataset for machine learning models (Fig. 1). The research protocols were approved by the ethics committees of both medical institutes.

2.2. Urinary-slide preparation for microscopic images

Urine samples were collected from the patients; 10 mL of each sample was centrifuged at 3000 rpm for 10 min, and the pellets were resuspended in 500 μL of the supernatant. The suspension was used to prepare slides for examination.

2.3. Training-database construction with urinary sediment images for deep neural network models

The flow of information for training dataset construction was described in Fig. 2. In brief, we processed each image using adaptive histogram equalization. Further, each original image was segmented for image augmentation; the positive segment images, background images of the positive cases, and negative segment images were categorized into positive or negative groups, in accordance with their role in machine-learning training.

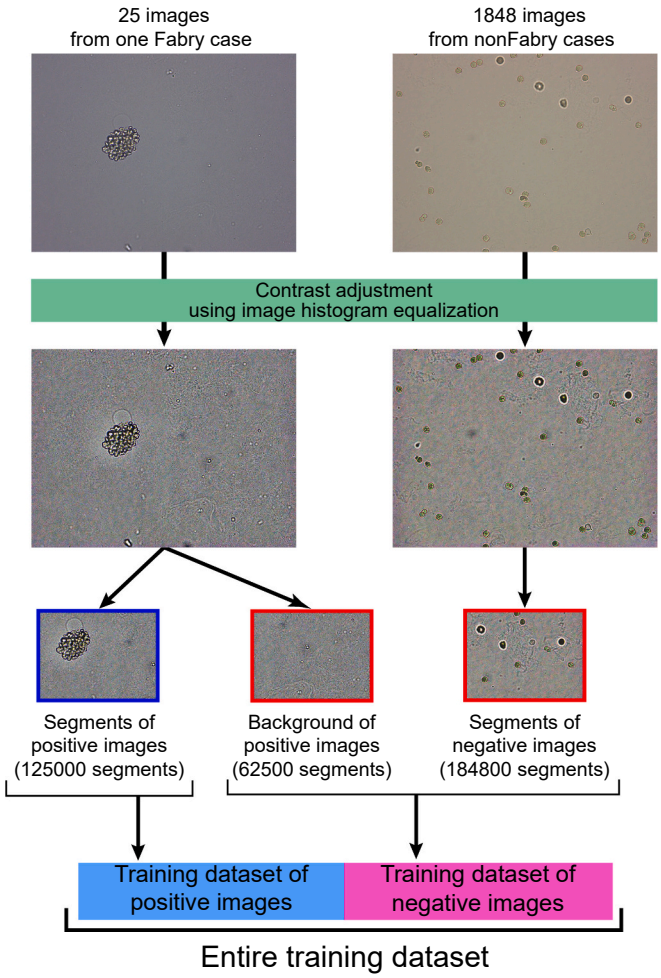

Fig. 2. Overview of the image preprocessing workflow for training datasets. Each image in the training group was first processed using histogram equalization for contrast adjustment, as shown in Fig. 3A. 1:4 scale-sized rectangles were randomly clipped from these images, as shown in Figs. 3B–3D. Among these processed segmented images, the segmented positive images were categorized as positive training datasets, while the negative segmented images and the background of the positive images were categorized as negative datasets. For training the neural network models, these datasets were randomly separated as three-fourth for training and one-fourth for hyper-parameter tuning.

In detail, after the digitalization, the contrast of each image was adjusted using adaptive histogram equalization (Fig. 3A). Image augmentation was then performed with image-trimming, as described below:

(I) One-fourth sized rectangles of the original urinary sediment images from Fabry cases were randomly set to include the center of the mulberry cells. The segmented image trimmed by each rectangle contained more than approximately a quarter of a single mulberry cell. These quarter-sized segmented images were defined as the positive segments and were categorized into positive training datasets. (Fig. 3B)

(II) One-fourth-sized rectangles of the original images from Fabry cases, which did not contain any mulberry cells, were randomly set. The segments trimmed by these rectangles were defined as the background segments and were categorized into negative training datasets. (Fig. 3C)

(III) One-fourth sized rectangles of the original images from non-Fabry cases were randomly set. These trimmed images were defined as negative segments and were categorized into negative training datasets. (Fig. 3D)

In the above processes ((I), (II), and (III)), image augmentation was performed by repeated random trimming of the quarter-sized rectangles. This database was mainly utilized for training each neural network model for the classification of the urine samples. The pathological diagnosis of each urinary sediment finding in the original images was performed by qualified medical staff (C.K., a medical technologist in St. Marianna), and confirmed by the medical doctor, who participated in this research (O.M.), during image processing.

2.4. Neural-network model training

The segmented images were converted into (192, 256, 3) vectors, before being input to the training machine-learning models. VGG19 [22] was used as the pre-trained deep convolutional neural network architecture for the convolutional layers. As the top layers, we connected self-made fully connected layers with batch normalization layers and dropout layers. Finally, a sigmoid function for binary classification was set as the output layer. The summary of the model was plotted in Supplementary Fig. 2. We continued training a model with each training dataset until its loss score reached a plateau or model overfitting occurred (Supplementary Fig. 3). A patience, the number of epochs to wait if no progress on the test dataset, was defined as 20. The maximal number of epochs for training was set as 300. The model with the lowest loss score was saved and evaluated with the validation dataset. Our models are already submitted in https://github.com/huryu/DL_Fabry. Those models can be performed in mid-range consumer computer systems with GPU and Python programming language.

2.5. Evaluation of the trained model

Cases other than those utilized for the training dataset were used as the validation dataset. Each of these images was processed with or without adaptive histogram equalization and divided into 4 × 4 quarter-sized rectangles, as shown in Fig. 4F. The findings in each segment were judged by medical staff (C.K. and O.M.) and categorized into a positive or negative group as pre-prediction categories. The segments that contained more than a quarter of a single mulberry cell was defined as positive and defined as negative if the segments did not contain any mulberry cells. The segments from Fabry cases, which included less than a quarter of a single mulberry cell, were excluded from this evaluation process. Then, the prediction of classification for these validation datasets by trained models was performed.

If the pre-prediction category matched the prediction result, the prediction was defined to be true; else, it was defined as false. The receiver operating characteristic (ROC) curves were constructed for each target findings by varying the threshold and plotting the true-positive rate (i.e., sensitivity) and false-positive rate (i.e.,

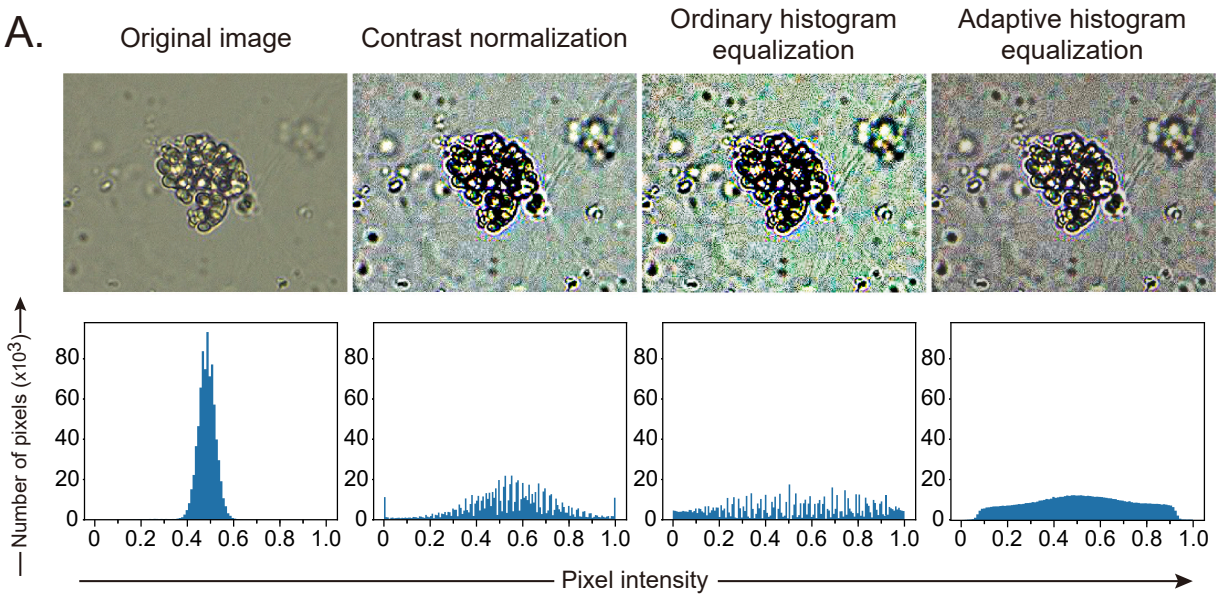

(caption on next page)

Fig. 3. Image preprocessing of the original images into segmented images.
(A) Representative images before and after equalization are shown in the upper row. Histograms of the pixel intensity before and after equalization are shown in the lower row. (B) Rectangular areas that were ¼ the size of the original image, including the center of the mulberry cells, were randomly clipped out for the positive training dataset. (C) As the positive-image backgrounds, rectangular areas that were ¼ the size of the original image and did not overlap any part of mulberry cells were randomly clipped out. (D) As negative segmented images, rectangular areas that were ¼ the size of the original image were randomly clipped out. The segmented images from (B) were incorporated into the positive dataset, whereas those from (C) and (D) were incorporated into the negative dataset for training the neural network, as shown in Fig. 2.

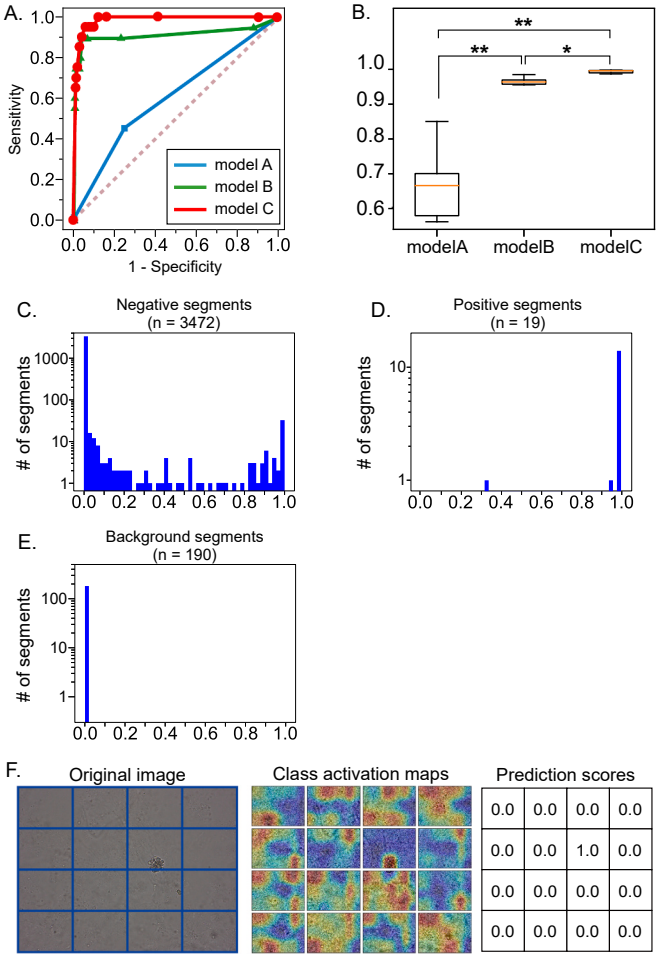

Fig. 4. Model evaluation based on each training dataset.
(A, B) Representative ROC curves (A) and boxplots of AUCs for each model (B) were shown (N = 15–25 per group, means ± standard error). *$p < .05$; **$p < .01$.
(C-E) Representative histograms of the scores for the negative (C), positive (D), and Fabry background segments (E), predicted with the model C. The intervals on the y-axis scale were logarithmically transformed.
(F) Visualization of the class activation area on the segmented images. The original urinary sediment images (left) were segmented and displayed as heatmaps according to the contribution of the model activation for classification (center). Each segment was processed using the models and converted to scores for Fabry disease prediction (right).

1–specificity) at each threshold. The areas under the ROC curves (AUCs) were computed to assess the classification algorithms. To detect the area based on which the models made their judgment, we have visualized the heatmaps of the class activation for each segmented image.

2.6. Statistical analysis

Mann-Whitney U tests were used to compare AUCs between each group, and analyses were performed using the SciPy, scikit-learn, and Keras/TensorFlow python packages, $p < .05$ was considered statistically significant.

2.7. Data handling

The image data were blinded and analyzed by H.U. The entire code is open to the public in GitHub (https://github.com/huryu/DL_Fabry).

2.8. Data availability

The datasets generated and/or analyzed during the current study are available from the corresponding author upon reasonable request.

3. Results

Three Fabry patients, whose diagnosis was definitely confirmed, were enrolled in this study as disease-positive cases. Further, 2065 nonFabry cases, whose urine sediment images were already stored in the laboratory database of the respective medical institution, were enrolled as negative controls after their clinical reports were reviewed to confirm that they did not exhibit any signs, symptoms, or other laboratory findings indicating the existence of Fabry disease. Briefly, these images were divided into training or validation group, preprocessed, and saved as each dataset, as shown in Fig. 1.

In detail, twenty-five urinary sediment slides obtained from one Fabry patient were included in the training dataset as positive images. 1848 cases were randomly selected from the negative control cases, and the urinary sediment images from each case were included in the negative training dataset. The main findings of negative control samples for training sets are summarised in Supplementary Table 1. From these original urine images, 125,000 positive segments, 62,500 background segments, and 184,800 negative segments were generated for the training dataset using image augmentation methods. From this dataset, three-fourth of the whole images were randomly selected for training, and the rest of the images were used for hyperparameter tuning. The models trained with this database were called ‘C’ models (Fig. 2).

For comparative purposes, training datasets without histogram equalization nor positive background sampling (Supplementary Fig. 1A), and ones without positive background sampling (Supplementary Fig. 1B) were also constructed. The neural network models trained with these datasets were called ‘A’ models and ‘B’ models, respectively.

For the validation dataset, fourteen images obtained from two Fabry patients, and 217 negative control images were used. All cases used in the validation dataset did not overlap with any cases used in the training dataset. From these original images, we obtained nineteen positive segments of the Fabry cases, 189 background segments, and 3472 negative segments (Fig. 1). With this validation dataset, we evaluated each model’s performance for its classification accuracy.

After the initial weights in each layer of the model were decided with the random initialization, these weights were gradually adjusted to decrease the loss score according to the backpropagation algorithm during model training (Supplementary Fig. 3). To confirm the robustness, we made several models based on each algorithm. These results are shown in Fig. 4A and B, and Supplementary Figs. 4A and 4B.

The ROC curves revealed that model A displayed only slight superiority, compared to random guessing (Fig. 4A). The construction of the training dataset with color-histogram-equalized images significantly improved the accuracy of the trained models (model B), compared to the

'A' models. Further improvement was observed when the backgrounds of the positive images were appended to the negative training dataset for model training (model C) (Fig. 4A). The AUCs for model C was significantly higher than model B, reflecting the accuracy of each model (0.968 +/− 0.004 vs 0.945 +/− 0.005; $p = .013$) (Fig. 4B).

The prediction scores for the negative segment images were distributed in the range 0–1.0, with extreme deviation to the zero points, when model C was used for prediction (Fig. 4C). The predicted scores of the Fabry-background images were concentrated around zero (Fig. 4E). The prediction scores of the positive segmented images were concentrated around 1.0, with model C (Fig. 4D). On the contrary, with the model B, the variance of the negative prediction scores was large, and the prediction scores of the background images were distributed in the range 0–1.0 (Supplementary Fig. 2). These findings suggest that only model C can successfully predict the urinary sediment images from Fabry cases based on the presence of mulberry cells. To confirm this hypothesis, we visualized the class activation heatmaps for these models. In these maps, when the model C judged the images as negative, the activated areas were disseminated over almost the entire area, but when they were detected as positive segment images, the activated areas of the heatmaps were concentrated only on the mulberry-cell images (Fig. 4F).

4. Discussion

Most of the Fabry cases display only nonspecific symptoms in their early stages, and these aspects disturb the early diagnosis of this disease [12,23]. Previous reports suggest that some therapeutic options may be useful to reduce the progression of Fabry disease if these are initiated before disease progression [17]. Thus, early diagnosis is critical for the timely application of therapeutic interventions. We focused on the existence of mulberry cells, the early signs of Fabry disease with high-sensitivity and high-specificity [20], when we constructed AI-based models to detect Fabry cases.

The expected pretest probability of Fabry disease is one in several thousand, which is considerably low in the general population [6–10]. This low prevalence leads to the substantial numbers of false-positive cases even with sufficiently accurate diagnostic tools. This aspect suggests that stringent specificity, rather than high sensitivity, is crucial for the screening system of Fabry disease.

In general, the large number of images is critical for the sufficient generalization of training dataset when we construct accurate neural network-based models [24]. This requirement could be a bottleneck when we build AI models for rare diseases because of their limited number of cases [21]. To attain enough generalization against the diversity of clinical sample images, we applied novel strategies to construct the training dataset from Fabry cases.

We performed the image augmentations of positive and negative samples to enhance the generalization of training image sets, as shown in Fig. 3B and D. The background segments from Fabry cases, which did not contain any signs of Fabry disease, were also amplified and added to the training dataset as a part of negative datasets (Fig. 3C).

For further improvement of generalization against all clinical input images, we transformed all the input images for training and validation datasets using histogram equalization for model B or model C. Negative background images were added to create Model C. Retraining with many negative images improved the specificity of correctly discriminating images with mulberry cells. In general, improvement of specificity contributes more to the expansion of the area under the ROC curve than sensitivity in our models. Although this conversion regulates the color diversity of the input images, this preservers the main contours of the mulberry cells, and contributes to the improvement of the performance of trained models (Figs. 3A, 4A, B).

To evaluate the combination of these strategies, we compared the performances of the models constructed with the different training datasets (models A, B, and C). A drastic improvement in the accuracy of model B was observed compared to the model A (Fig. 4A and B). Further, the model performances significantly increased when we added the background images of Fabry cases to the negative training dataset (model C, Fig. 4A, and B). Comparing the prediction score distributions of model Cs (Fig. 4C) with model Bs (Supplementary Fig. 2), we could conclude that background segments are useful to reduce the number of false-positive segments. Also, the distribution of the image scores (Figs. 4C-4E) and the class activation maps (Fig. 4F) in model C indicated that this model could predict each segment's score based on the existence of mulberry cells.

Consequently, we could construct the models that predict the presence or absence of mulberry cells in urinary samples with high accuracy, despite the small number of original images for training datasets. The results of model prediction were easily interpreted by human cognition, leading to further elimination of false-positive cases.

Thus, we developed high-sensitivity and high-specificity machine learning models, which can classify the disease-specific findings from numerous samples. Combined with the final human judgments, this model could be utilized as a rapid, low-cost universal screening system for Fabry patients. In the future, we expect that these classifier systems, which include both machine and human recognition, for detecting urinary sediment, would be extensively used for detecting other inborn metabolism disorders.

Author contributions

Hidetaka Uryu conceived and designed the study, developed the algorithms, validated the constructed models, performed the statistical analysis, and drafted the initial manuscript.

Ohsuke Migita conceived and designed the study, and drafted the initial manuscript.

Minami Ozawa collected, anonymized, and analyzed the data from the National Center for Child Health and Development (NCCHD) or St. Marianna University School of Medicine.

Chieko Kamijo collected, anonymized, and analyzed the data from St. Marianna University School of Medicine.

Saki Aoto collected, anonymized, and analyzed the data from NCCHD or St. Marianna University School of Medicine.

Kohji Okamura collected, anonymized, and analyzed the data from NCCHD.

Fuyuki Hasegawa collected, anonymized, and analyzed the data from NCCHD.

Yoko Kishimoto-Narumi collected, anonymized, and analyzed the data from NCCHD.

Torayuki Okuyama collected, anonymized, and analyzed the data from NCCHD.

Motomichi Kosuga collected, anonymized, and analyzed the data from NCCHD.

Kenichiro Hata conceived and designed the study.

Funding

This study was supported by the Research & Development grant from the National Center for Child Health and Development (Grant 30-37).

Ethics approval

All procedures followed were in accordance with the ethical standards of the responsible committee on human experimentation (institutional and national) and with the Helsinki Declaration of 1975, as revised in 2000. The research protocols were approved by the ethics committees of both the National Center for Child Health and Development and St. Marianna University School of Medicine. All patients (or their guardians) approved of the possible use of their left-over samples for method validation purposes, in agreement with institutional and national legislation. This article does not contain any studies with

animal subjects performed by any of the authors.

Declaration of Competing Interest

All authors have no conflict of interest to declare.

Data availability

Data will be made available on request.

Acknowledgments

This study was supported by the R & D grant (30-37 to H.U.) from the National Center for Child Health and Development (Tokyo, Japan), and Health, Labour and Welfare Sciences Research Grants (20FC1034).

Appendix A. Supplementary data

Supplementary data to this article can be found online at https://doi.org/10.1016/j.ymgmr.2022.100921.

References

[1] D.F. Bishop, R. Kornreich, R.J. Desnick, Structural organization of the human alpha-galactosidase A gene: further evidence for the absence of a 3′ untranslated region, Proc. Natl. Acad. Sci. U. S. A. 85 (1988) 3903–3907. https://www.pnas.org/doi/abs/10.1073/pnas.85.11.3903.

[2] D.P. Germain, Fabry disease, Orphanet. J. Rare Dis. 5 (2010) 30. https://ojrd.biomedcentral.com/articles/10.1186/1750-1172-5-30.

[3] M.D. Sanchez-Nino, A.B. Sanz, S. Carrasco, et al., Globotriaosylsphingosine actions on human glomerular podocytes: implications for Fabry nephropathy, Nephrol. Dial. Transplant. 26 (2011) 1797–1802, https://doi.org/10.1093/ndt/gfq306.

[4] R.O. Brady, A.E. Gal, R.M. Bradley, et al., Enzymatic defect in Fabry's disease. Ceramidetrihexosidase deficiency, N. Engl. J. Med. 276 (1967) 1163–1167. https://www.nejm.org/doi/full/10.1056/NEJM196705252762101.

[5] M.H. Branton, R. Schiffmann, S.G. Sabnis, et al., Natural history of Fabry renal disease: influence of alpha-galactosidase A activity and genetic mutations on clinical course, Medicine 81 (2002) 122–138, https://doi.org/10.1097/00005792-200203000-00003.

[6] P.J. Meikle, J.J. Hopwood, A.E. Clague, W.F. Carey, Prevalence of lysosomal storage disorders, JAMA 281 (1999) 249–254, https://doi.org/10.1001/jama.281.3.249.

[7] M. Spada, S. Pagliardini, M. Yasuda, et al., High incidence of later-onset fabry disease revealed by newborn screening, Am. J. Hum. Genet. 79 (2006) 31–40, https://doi.org/10.1086/504601.

[8] W.L. Hwu, Y.H. Chien, N.C. Lee, et al., Newborn screening for Fabry disease in Taiwan reveals a high incidence of the later-onset GLA mutation c.936+919G>A (IVS4+919G>A), Hum. Mutat. 30 (2009) 1397–1405, https://doi.org/10.1002/humu.21074.

[9] T.P. Mechtler, S. Stary, T.F. Metz, et al., Neonatal screening for lysosomal storage disorders: feasibility and incidence from a nationwide study in Austria, Lancet. 379 (2012) 335–341, https://doi.org/10.1016/s0140-6736(11)61266-x.

[10] T. Inoue, K. Hattori, K. Ihara, et al., Newborn screening for Fabry disease in Japan: prevalence and genotypes of Fabry disease in a pilot study, J. Hum. Genet. 58 (2013) 548–552, https://doi.org/10.1038/jhg.2013.48.

[11] R.J. Desnick, R. Brady, J. Barranger, et al., Fabry disease, an under-recognized multisystemic disorder: expert recommendations for diagnosis, management, and enzyme replacement therapy, Ann. Intern. Med. 138 (2003) 338–346, https://doi.org/10.7326/0003-4819-138-4-200302180-00014.

[12] A. Mehta, R. Ricci, U. Widmer, et al., Fabry disease defined: baseline clinical manifestations of 366 patients in the Fabry outcome survey, Eur. J. Clin. Investig. 34 (2004) 236–242, https://doi.org/10.1111/j.1365-2362.2004.01309.x.

[13] R. Schiffmann, G.J. Murray, D. Treco, et al., Infusion of alpha-galactosidase a reduces tissue globotriaosylceramide storage in patients with Fabry disease, Proc. Natl. Acad. Sci. U. S. A. 97 (2000) 365–370, https://doi.org/10.1073/pnas.97.1.365.

[14] R. Schiffmann, J.B. Kopp, H.A. Austin 3rd, et al., Enzyme replacement therapy in Fabry disease: a randomized controlled trial, JAMA. 285 (2001) 2743–2749, https://doi.org/10.1001/jama.285.21.2743.

[15] D.P. Germain, D.A. Hughes, K. Nicholls, et al., Treatment of Fabry's disease with the pharmacologic chaperone Migalastat, N. Engl. J. Med. 375 (2016) 545–555, https://doi.org/10.1056/nejmoa1510198.

[16] M. Banikazemi, J. Bultas, S. Waldek, et al., Agalsidase-beta therapy for advanced Fabry disease: a randomized trial, Ann. Intern. Med. 146 (2007) 77–86, https://doi.org/10.7326/0003-4819-146-2-200701160-00148.

[17] A. Ortiz, A. Abiose, D.G. Bichet, et al., Time to treatment benefit for adult patients with Fabry disease receiving agalsidase beta: data from the Fabry registry, J. Med. Genet. 53 (2016) 495–502, https://doi.org/10.1136/jmedgenet-2015-103486.

[18] H. Shimohata, Y. Ogawa, H. Maruyama, et al., Renal variant of Fabry disease diagnosed by the presence of urinary mulberry cells, Intern. Med. 55 (2016) 3475–3478, https://doi.org/10.2169/internalmedicine.55.7367.

[19] T. Nakamichi, M. Miyazaki, K. Nakayama, et al., Fabry's disease discovered with chance urinary mulberry cells: a case report, CEN Case Rep. 2 (2012) 49–52, https://doi.org/10.1007/s13730-012-0038-x.

[20] M. Selvarajah, K. Nicholls, T.D. Hewitson, G.J. Becker, Targeted urine microscopy in Anderson-Fabry disease: a cheap, sensitive and specific diagnostic technique, Nephrol. Dial. Transplant. 26 (2011) 3195–3202, https://doi.org/10.1093/ndt/gfr084.

[21] C. Faviez, X. Chen, N. Garcelon, et al., Diagnosis Support Systems for Rare Diseases: A Scoping Review vol. 15, 2020, p. 94, https://doi.org/10.1186/s13023-020-01374-z.

[22] K. Simonyan, A. Zisserman, Very Deep Convolutional Networks for Large-Scale Image Recognition, eprint arXiv:1409.1556, https://ui.adsabs.harvard.edu/abs/2014arXiv1409.1556S, 2014.

[23] M. Arends, C. Wanner, D. Hughes, et al., Characterization of classical and nonclassical Fabry disease: a multicenter study, J. Am. Soc. Nephrol. 28 (2017) 1631–1641, https://doi.org/10.1681/asn.2016090964.

[24] R. Geirhos, C.R. Medina Temme, J. Rauber, H.H. Schütt, F. Bethge, F.A. Wichmann, Generalisation in Humans and Deep Neural Networks, eprint arXiv:1808.08750, https://ui.adsabs.harvard.edu/abs/2018arXiv180808750G, 2018.